JOURNAL OF CATALYSIS **158,** 128–141 (1996)
ARTICLE NO. 0014

Study of a New Iron Phosphate Catalyst for Oxidative Dehydrogenation of Isobutyric Acid

P. Bonnet, J. M. M. Millet, C. Leclercq, and J. C. Védrine

Institut de Recherches sur la Catalyse, CNRS, associé a l'Université Claude-Bernard, Lyon I, 2 avenue A. Einstein, F-69626 Villeurbanne Cedex, France

Received May 23, 1995; revised August 24, 1995; accepted August 29, 1995

A new method of preparation of iron phosphate-based catalysts has been developed. The catalysts obtained are characterized by a single phase which is very active and selective in methacrylic acid (MAA) formation. This phase, identified as $Fe_2(PO_3OH)P_2O_7$, is an selective but much more active than industrial iron phosphate-based catalysts prepared by another method. The similarities between the catalytic properties of this phase and the active phase of the industrial catalyst ($\alpha Fe_3(P_2O_7)_2$ which is superficially oxidized and hydrated to the form $Fe_{3-x}^{3+}Fe_x^{2+}(PO_3OH)_{3+x}(PO_4)_{1-x}$) support the role of the different species previously proposed especially the important role of the PO_3OH groups and of the clusters of face-sharing Fe–O octahedra (7, 25). These clusters correspond to dimers $(Fe_2O_9)^{13-}$ in $Fe_2(PO_3OH)P_2O_7$, whereas they correspond to trimers $(Fe_3O_{12})^{16-}$ in the active phase of industrial catalysts. However, a reduced amorphous phase has been shown to form at the surface of the $Fe_2(PO_3OH)P_2O_7$ phase which may contain the same species as the active phase of the industrial catalyst, explaining in this way the similarities observed in the catalytic properties. The greater activity of the new catalysts can be explained by the fact that the industrial catalysts contained not only the $\alpha Fe_3(P_2O_7)_2$ phase but other inactive phases. The role attributed to water in shifting the hydration equilibrium and stabilizing superficially the $Fe_3(PO_3OH)_3PO_4$ phase is confirmed. Finally, it appears that the new catalysts are hydrated in the bulk rather than only on the surface as was the case for $\alpha Fe_3(P_2O_7)_2$ and this is likely to have a direct effect on the ability of the solid to hydrate more easily, allowing a stabilization of the catalytic properties at lower partial pressures of water or even in the absence of added water.

INTRODUCTION

Iron phosphorus mixed oxides are known to selectively catalyze the oxidative dehydrogenation of isobutyric acid (IBA) to methacrylic acid (MAA). Two methods of preparing these catalysts have been published. The most common method (method 1) which is reported in almost all the patent literature (1–4) consists of mixing a ferric compound (generally a nitrate) dissolved in water with an aqueous solution of phosphoric acid. The mixture is evaporated, dried, and calcined between 673 and 773 K in a stream of flowing air. Most of the time, alkaline metals are added to the solution in the form of nitrates. The more efficient catalysts were obtained with the addition of cesium and had Fe/P/Cs atomic ratios around 1/1.2/0.1 (3). The second method of synthesis (method 2) was described recently by Ai *et al.* (5). It consists of preparing an iron hydroxide gel from a dilute ammonia solution containing iron nitrate and then allowing this gel to react with an aqueous solution of orthophosphoric acid under boiling conditions. In both methods colloidal silica was added to the mixtures.

The two methods described gave precursors which were totally transformed under the conditions of catalysis which led to mixtures of several phases. In the case of catalysts prepared using method 1, we showed previously that among the phases formed, the more active and selective one was a mixed valence iron pyrophosphate $\alpha Fe_3(P_2O_7)_2$ (6, 7). The X-ray diffraction patterns of the catalysts prepared by Ai and co-workers using method 2 also contained such a phase after the catalytic test. However the authors referred to it as a Y phase and suggested also that it may be the active phase of these catalysts (8). Along with this very active and selective phase other phases such as $CsFeP_2O_7$ (method 1), $\beta Fe_3(P_2O_7)_2$ (method 2), $FePO_4$, and $Fe_2P_2O_7$ (methods 1 and 2) were formed. These phases were shown to be much less selective and active and to play only a minor role in the reaction (9, 10). In the present work we have attempted to study a new method of preparation of iron phosphate catalysts that avoids the formation of the inactive phases in the mixture in order to yield highly active and selective catalysts.

EXPERIMENTAL

Iron phosphate catalyst syntheses were carried out by reacting vivianite and $H_4P_2O_7$ in acetone under reflux. Vivianite is a hydrated ferrous iron phosphate $Fe_3(PO_4)_2 \cdot 8H_2O$ prepared by mixing deoxygenated aqueous solutions of $Fe(NH_4)_2SO_4 \cdot 6H_2O$ and Na_2HPO_4 with

0021-9517/96 $12.00

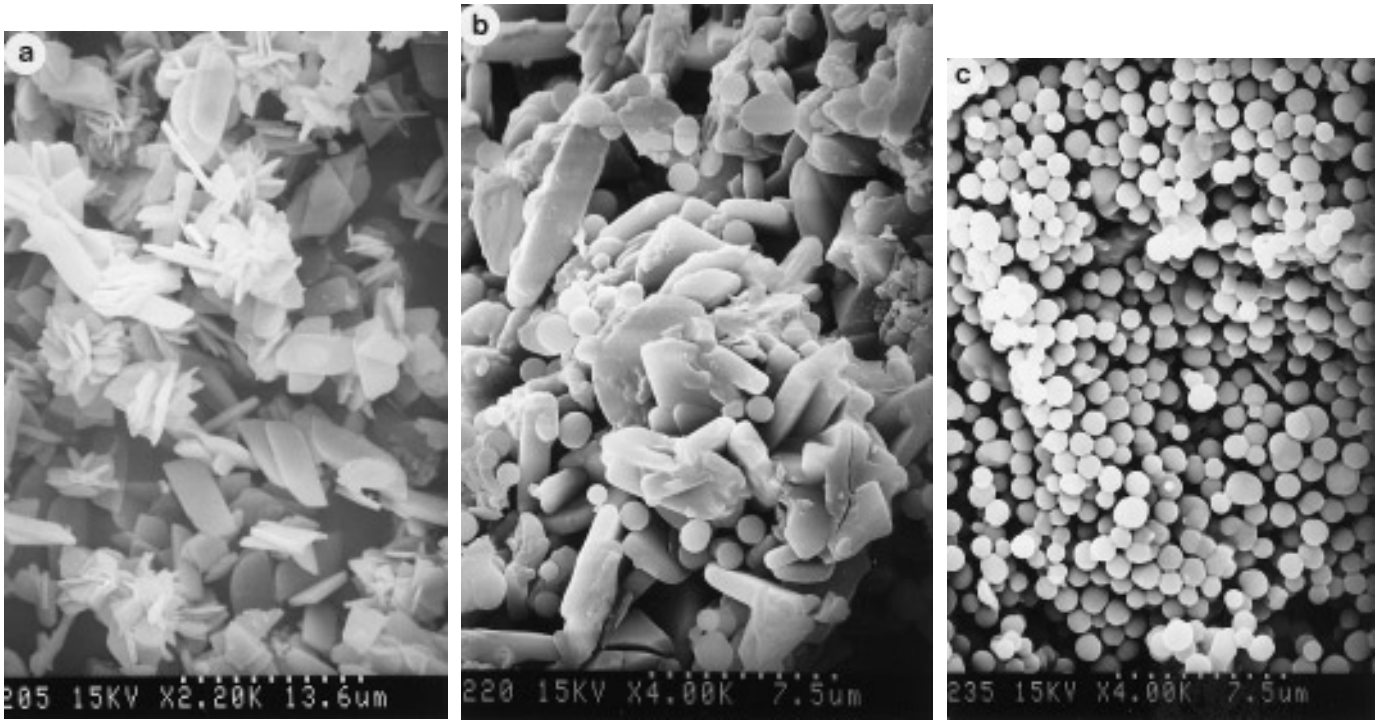

FIG. 1. Scanning electron micrographs of the vivianite before (a), during (b), and after (c) synthesis.

CH_3COONa under argon. The precipitate formed during stirring was allowed to settle for 2 days before filtration, washed by deoxygenated water, and evaporated to dryness under vacuum. The iron phosphate catalyst synthesis reaction was carried out in a 250 cm^3 flask equipped with a mechanical stirrer and a reflux condenser. The reactant P/Fe ratio varied between 1.5 and 4.5 by use of the appropriate amounts of pyrophosphoric acid. The duration of the reaction was usually 15 h. After completion of the reaction, the solid phases were filtered, washed with acetone, and dried at 313 K in air. A catalyst prepared using the method 1 was supplied by the company ELF ATOCHEM (3); it will be designated as the industrial catalyst.

Powder X-ray diffraction patterns were obtained using a Siemens D500 diffractometer and Cu$K\alpha$ radiation. They were recorded with 0.02° (2θ) steps over the 10–88° angular range with 1 s or in some cases 16 s counting time per step. The data obtained from the powder patterns have been used to calculate the unit cell of the compounds using a method proposed by De Wolff (11). From a series of patterns, obtained with different vivianite contents, an estimation of the quantity of the latter phase was established by comparing the intensities of the main diffraction peak of the vivianite (0, 2, 0) to that of the main diffraction peak of pure vivianite. The iron and phosphorus contents were quantitatively determined by atomic absorption and specific surface areas were determined by the BET method using nitrogen adsorption. ^{57}Fe Mössbauer spectroscopy was performed at 298 K as previously described (12). TGA experiments were performed using a SETARAM TGA-DTA 92 thermobalance coupled to a Balzers 420 QMC mass spectrometer (13). EDX analyses were performed with a scanning electron microscope JEOL 840A LGS (0.2-40 kV), fitted with an energy dispersive X-ray spectrometer TRACOR Si(Li) detector with Be or ultrathin window and TN 5422 analyzer. Observations by electron microscopy were also performed in a conventional transmission electron microscope JEOL JEM 2010 (200 kV) in a high resolution configuration (resolution picture point: 0.194 nm), filtered with an energy dispersive X-ray spectrometer (PENTAFET detector + LINK ISIS analyzer system). With this microscope, it was possible to obtain very small electron probes (≥1 nm) to perform X-ray and electron diffraction studies. XPS measurements were performed with a VG ESCALAB 200 R. Charging of catalysts samples was corrected by setting the binding energy of adventitious carbon (C^{1s}) at 284.5 eV. Qualitative analysis of the peaks, in terms of elemental ratios, was carried out as described previously (14). The experimental precision on XPS quantitative measurements was considered to be around 20%.

Characterization of the samples was performed before and after catalytic test. After catalytic test, the catalysts were recovered by cooling them down rapidly under flowing nitrogen. Most of the characterization of the samples

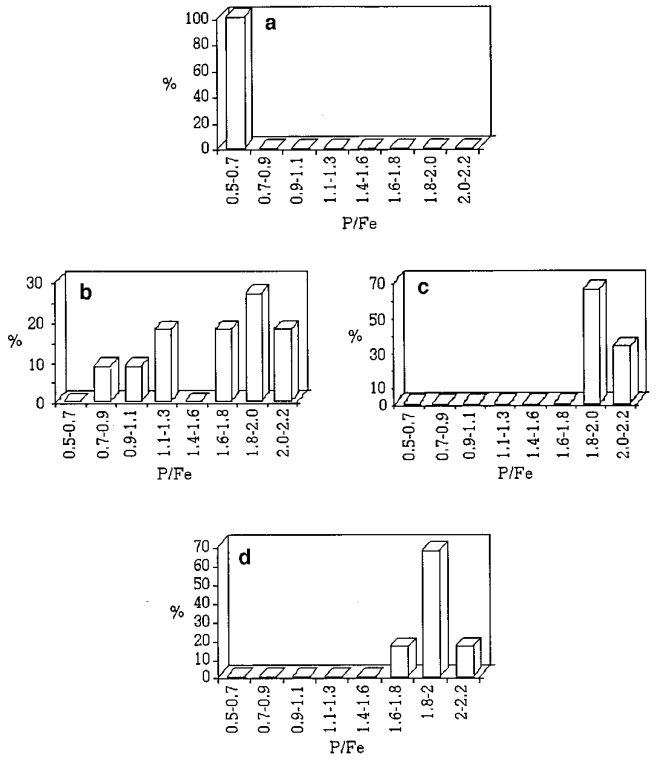

FIG. 2. Distribution of the P/Fe ratio determined from microanalysis of the vivianite platelets before (a) and at an intermediate stage during the course of the synthesis reaction (b) and of the disk-shape particles observed at an intermediate stage during the course of the synthesis (c) and after its completion (d).

before catalysis was performed on the solids after synthesis just prior to the catalytic run. However, in order to follow the transformation of the starting solids, these solids have been analyzed by the different techniques before and after the completion of the synthesis as well as at an intermediate stage during the course of the synthesis reaction. To achieve the intermediate characterization, the synthesis reaction was stopped after 10 h and the solids were recovered as described for the completion of the reaction.

The oxidative dehydrogenation of IBA to MAA was carried out at atmospheric pressure in a dynamic differential microreactor containing 30 to 50 mg of catalyst (15). Reaction conditions were as follows: total flow rate 1 $cm^3 \cdot s^{-1}$; reaction temperature 658 K; $O_2/IBA/H_2O/N_2$: 4.26/5.86/72.0/19.2 kPa. The catalysts were compared using these conditions, with different masses in order to keep a comparable conversion level of about 20%. To study the effect of the water partial pressure the oxygen and IBA partial pressures were kept constant at 4.26 and 5.86 kPa, respectively, and the water partial pressure was varied from 0 to 72.0 kPa. Propene, acetone, and CO_2 were the three byproducts formed with methacrylic acid under our reaction conditions (15).

RESULTS

1. Synthesis and Characterization of the Catalyst Precursors

During the synthesis, the vivianite slowly changed color from blue to grey but remained insoluble in acetone. In order to follow the transformation of the vivianite, the solid was studied by scanning electron microscopy (SEM) coupled with microanalysis, X-ray diffraction, and chemical analysis before, at an intermediate stage, and after the synthesis reaction.

The starting vivianite presented a morphology of thin platelets (Fig. 1a) with a well-defined and uniform distribution of the P/Fe ratio in accordance with the chemical analysis (P/Fe = 0.66) (Fig. 2a). The vivianite was well crystallized (Fig. 3a) and its extent of oxidation $Fe^{3+}/(Fe^{2+} + Fe^{3+})$, determined by Mössbauer spectroscopy, was equal to 20%. This oxidation state was in agreement with previous studies which showed that it was difficult to obtain it in its nonoxidized state (16, 17). After 10 h of reaction the SEM micrographs showed, besides the platelets, uniformly-sized, well-defined disk-like particles which seemed to be formed within the platelets (Fig. 1b). These

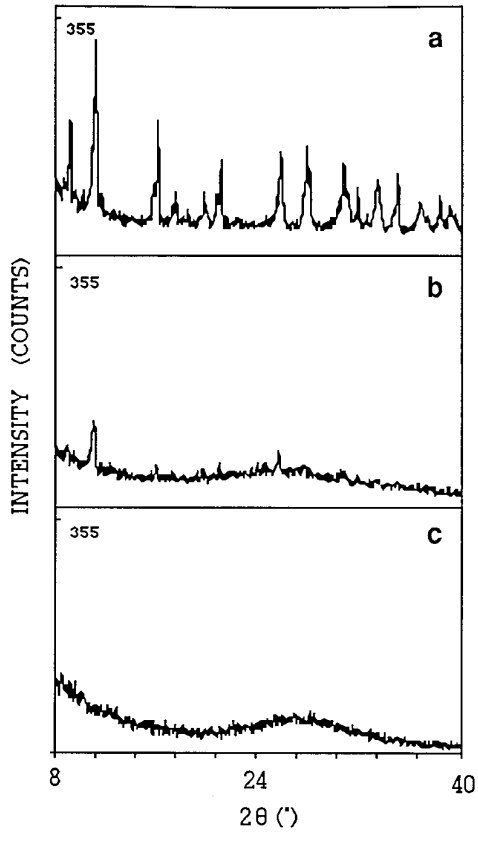

FIG. 3. X-ray diffraction patterns of the vivianite before (a), during (b), and after (c) synthesis.

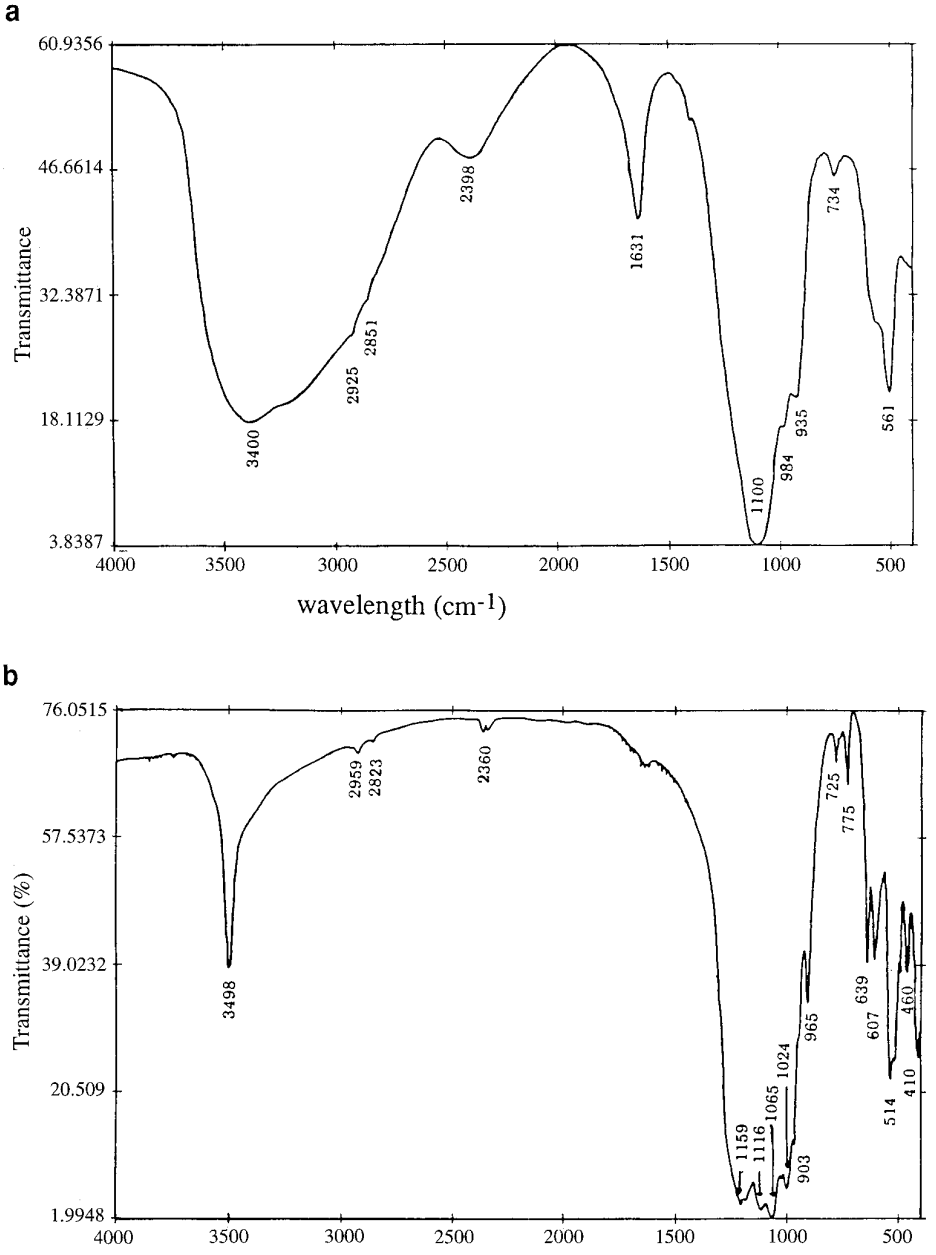

FIG. 4. Infrared spectra of the solid after synthesis (a) and after the catalytic test (b).

particles presented a relatively uniform composition ($1.8 < P/Fe < 2.3$) whereas that of the platelets became less uniform ($0.7 < P/Fe < 2.2$) (Fig. 2b). The chemical analysis gave a P/Fe ratio equal to 1.9, comparable to the microanalysis. The X-ray diffraction pattern showed the formation of an amorphous phase along with the peaks corresponding to the vivianite (Fig. 3b). The extent of oxidation increased to 70%. At the end of the reaction the solid obtained was only made up of completely amorphous particles of a disk-like shape, with an oxidation state equal to 80%. (Figs. 1c and 3c). The microanalysis gave a P/Fe ratio ranging from 1.8 to 2.3, slightly less than the chemical analysis which gave a value of 2.3 (Fig. 2c).

As a general feature, the specific surface areas of the solids obtained with different synthesis experiments ranged from 1 to 3 $m^2 \cdot g^{-1}$. They were lower than those determined for the starting vivianite (3–5 $m^2 \cdot g^{-1}$). The infrared spectrum of these solids after synthesis presented two regions of absorption (Fig. 4) and (Table 1). The first region, around 3400 cm^{-1}, corresponded to the hydroxyl groups from water molecules. The other region, between 1200 and 550 cm^{-1}, corresponded to symmetrical and asymmetrical

TABLE 1

IR Bands Attribution for the Spectra of the New Catalysts before and after Catalysis

Before catalysis		After catalysis	
Band (cm^{-1})	Attribution	Band (cm^{-1})	Attribution
3400	ν(OH) H_2O	3498	ν(P–OH)
2925	ν(CH) solvent	2959	ν(C–H) solvent
2851	ν(CH) solvent	2360	ν(C–O) CO_2
2398	ν(OH) $H_xP_2O_7$ or H_xPO_4	2823	ν(C–H) solvent
1631	OH H_2O	1159	ν(O–H) H_2O
1100	$\nu(PO_3)$	1116	$\nu(PO_3)$
984	$\nu(PO_3)$	1065	$\nu(PO_3)$
935	ν_{as}(POP)	1024	$\nu(PO_3)$
734	ν_{as}(POP)	1000	$\nu(PO_3)$
610	$\delta(PO_3)$	965	ν_{as}(POP)
516	$\delta(PO_3)$	903	ν(P–OH)
		775	ν_{as}(POP)
		725	ν_{as}(POP)
		639	$\delta(PO_3)$
		607	$\delta(PO_3)$
		514	$\delta(PO_3)$
		460	$\delta(PO_3)$
		410	$\delta(PO_3)$

vibrations of the phosphate groups. Among the bands corresponding to these vibrations, the two at 734 and 935 cm^{-1} corresponded to symmetrical and asymmetrical vibrations of P–O–P groups, respectively. The broad band at 2400 cm^{-1} was characteristic of the OH stretching of the POH group in acidic phosphates $H_xP_2O_7$ or H_xPO_4 (18, 19). Finally, the two weak bands at 2835 and 2951 cm^{-1} could be attributed to CH vibrations, likely related to residual acetone.

The thermogravimetric analyses of the solids under argon showed several weight losses between 373 and 873 K identified as due to water loss by mass spectrometry analysis. The total weight loss corresponded to 17.5% of the initial weight and the major reduction in weight (11% of the total) took place between 373 and 463 K. The solid thus contained less water than the starting vivianite (28%). The Mössbauer spectra of the samples were fitted with three doublets, two ferric and one ferrous, except for the samples in a highly reduced state for which another ferrous doublet was observed (20). For example, the spectrum of the precursor which was used for the catalytic test and the Mössbauer parameters calculated from its fit are presented in Fig. 5 and Table 2. The values of the isomer shifts and the quadrupolar splittings were characteristic of ferric and ferrous cations in relatively symmetrical octahedral environments. It was also observed that the ratio of the first ferric doublets to the sum of the second and the ferrous doublets, was always approximately equal to 60 : 40 which suggests that two types of sites exist in the precursors. XPS analysis of a standard precursor showed the presence of an excess of phosphorus on the surface compared to the bulk. The P/O ratios were greater than 0.25 which could be due to the presence of polyphosphate anions on the surface.

2. *Effect of Synthesis Parameters*

The effect of several parameters on the characteristics of the precursors obtained was studied. These parameters included the P/Fe reactant ratio, the nature of the solvent and of phosphorus acid, the reflux rate, and the reflux atmosphere.

2.1. Effect of the P/Fe reactant ratio. Syntheses with starting P/Fe ratio values varying from 1.5 to 4.5 were conducted under the same conditions. Elemental analysis indicated that the P/Fe ratio of the precursor increased with reactant P/Fe ratio (Table 3). The X-ray diffraction patterns of the samples showed that a reactant P/Fe ratio equal to 4.5 was needed in order to have complete transformation of the vivianite (Fig. 6). The quantity of vivianite in the samples has been calculated from X-ray diffraction data and from chemical analyses assuming, in the latter case, a P/Fe ratio equal to 0.66 for the unreacted vivianite and a P/Fe ratio equal to 2.3 for the amorphous phase. The study by Mössbauer spectroscopy of the samples showed that the oxidation extent increased with the P/Fe ratio (Table 4). This oxidation extent was compared to those calculated considering the phase content as deduced from chemical analyses data and oxidation extents of 82 and 20% for the amorphous and vivianite phases (Table 4). This comparison, which showed a good agreement between the experimental and calculated extents, indicated that the P/Fe ratio only affected the amount of vivianite transformed.

2.2. Effect of the rate of reflux and of the reflux atmosphere. The effect of the rate of reflux was studied by varying the temperature of the heating source between 348 and 573 K. The starting P/Fe ratio was maintained at 4.5 for all the preparations. All the samples prepared were amorphous to X-rays and presented the same P/Fe ratio (2.3). They only differed in their oxidation extent. It was observed that as the reflux rate increased, the oxidation extent of the samples decreased (Fig. 7). The reaction was also conducted at the same temperature of the heating source but under a flow of deoxygenated argon. No change was observed in the reaction products and in particular in its oxidation extent.

2.3. Effect of the nature of solvent and phosphoric acid. To study the effect of the solvent, the reaction was conducted in solvents as different as water, isopropanol, and toluene. In water the vivianite was transformed giving

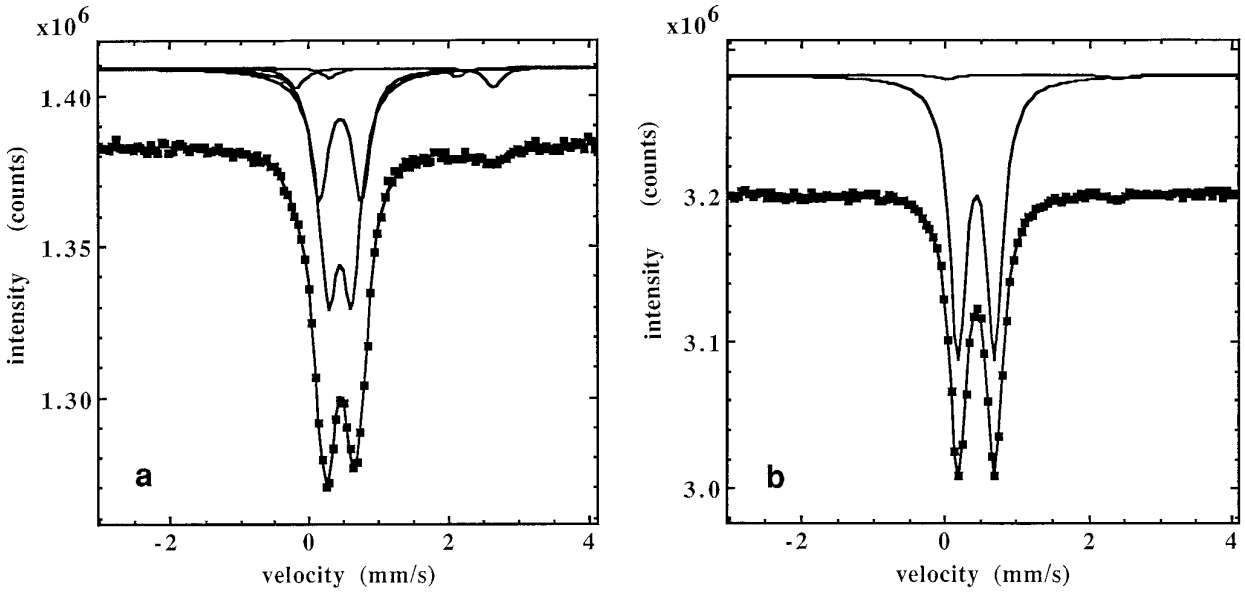

FIG. 5. Experimental Mössbauer spectra of a solid after synthesis (a) and after the catalytic test (b), recorded at 295 K. Solid lines are derived from least-square fits.

a mixture of phases among which only $FePO_4 \cdot 2H_2O$ was identified. In isopropanol the vivianite did not react. In toluene the pyrophosphoric acid was only slightly soluble which enabled us to use this solvent. Syntheses have also been performed under the same conditions but by using orthophosphoric acid instead of pyrophosphoric acid. In the presence of orthophosphoric acid, the vivianite underwent a transformation giving rise to a partially crystallized solid which has not been identified yet.

3. Catalyst Activation

The oxidative dehydrogenation of IBA was performed using as catalysts different synthesized solids and the industrial catalyst, under the conditions described in the Experimental section. Whereas high and stable performances were obtained in less than 2 h with the industrial catalyst. 2 days were needed with the synthesized solids. During this activation period a complete modification of the solids took place and a new phase, $Fe_2(PO_3OH)P_2O_7$, was formed from the synthesized solids. This phase was the only crystallized phase formed except in some cases where $\alpha Fe_3(P_2O_7)_2$ and $\beta Fe_3(P_2O_7)_2$ were also observed. In this article only the results obtained with samples giving only $Fe_2(PO_3OH)P_2O_7$ are reported. The samples were prepared with a starting P/Fe ratio equal to 4.5 with a temperature of the heating source of 348 K, which led to solids completely amorphous with a P/Fe ratio of 2.3 and oxidation level of 94%.

TABLE 2

Mössbauer Parameters Computed from the Spectrum of a Synthesized Precursor before and after Catalytic Reaction

Precursor	Sites	δ^a	W^b ($mm \cdot s^{-1}$)	δ^c	Relative intensity (%)
Before catalytic reaction	Fe^{3+}	0.44	0.32	0.34	61
	Fe^{3+}	0.45	0.30	0.61	33
	Fe^{2+}	1.20	0.26	1.83	2
	Fe^{2+}	1.22	0.30	2.82	5
After catalytic reaction	Fe^{3+}	0.44	0.28	0.51	98
	Fe^{2+}	1.19	0.26	2.37	2

[a] Isomer shift (given with respect to α-Fe).
[b] Line width.
[c] Quadrupolar splitting.

4. Catalytic Performances of the Catalysts

The results obtained from a precursor and an industrial type catalyst for the oxidative dehydrogenation of IBA were compared (Table 5). The new catalyst presented product selectivities comparable to those obtained with the industrial catalyst, but the selectivity to MAA was slightly higher. The new catalyst also appeared to be four times more active than the industrial catalyst per m^2.

4.1. Effect of the water partial pressure. The effect of the water partial pressure on the catalytic properties of the new catalyst was studied and compared to that of an industrial catalyst which was reported in previous studies (20, 21). To achieve a better comparison, a new term R has been defined as the ratio of the rate of MAA formation to the maximum of MAA formation obtained under the

conditions where the effect of water partial pressure was examined. Then for each catalyst, R was plotted as a function of the H_2O/IBA ratio (Fig. 8). Similar to the industrial catalyst, water partial pressure had a significant effect on the activity of $Fe_2(PO_3OH)P_2O_7$ especially at low partial pressure where the activity of the catalyst was significantly lower. At the same time the selectivities to MAA decreased and those of acetone and CO_2 increased with increasing H_2O partial pressure in a similar manner for the two catalysts (20). Unlike the industrial catalyst which had no activity when there was no water in the feed, the new catalyst retained a significant level of activity even in the absence of water. In order to study the stability of the new catalyst under catalytic reaction conditions without water, the water feed (72 kPa) was stopped and the performances of the catalyst were analyzed for 68 h; after this period the water partial pressure was reestablished. The ratio of the rate of formation of MAA to the initial rate decreased rapidly at the beginning and then decreased only very slowly (Fig. 9). The selectivity to MAA dropped to 61% and the rate of MAA formation dropped to 40% of the initial activity. When the water partial pressure was reestablished the catalyst displayed its initial MAA selectivity but not its initial activity since the rate of formation of MAA reached only 65% of the initial rate.

4.2. Effect of the oxygen and isobutyric acid partial pressure. The effect of the oxygen and IBA partial pressures in the feed on both the formation rates of the reaction products and their selectivity was studied and is reported in Figs. 10 and 11. The formation rates of MAA, acetone, and CO_2 increased with the partial pressures of IBA and oxygen, whereas that of propene was not significantly affected. In terms of selectivity, the increase of IBA partial pressure led to higher MAA selectivity and lower acetone and CO_2 selectivities and the increase in oxygen partial pressure led to the opposite. Kinetic orders relative to oxygen and IBA for the formation of MAA, acetone, and propene have been calculated (Table 6). They were not integer values and they were close to those calculated for the industrial catalyst. This suggests that the IBA was activated through an adsorbed species (20) and that the same mechanism could be involved in both types of catalysts.

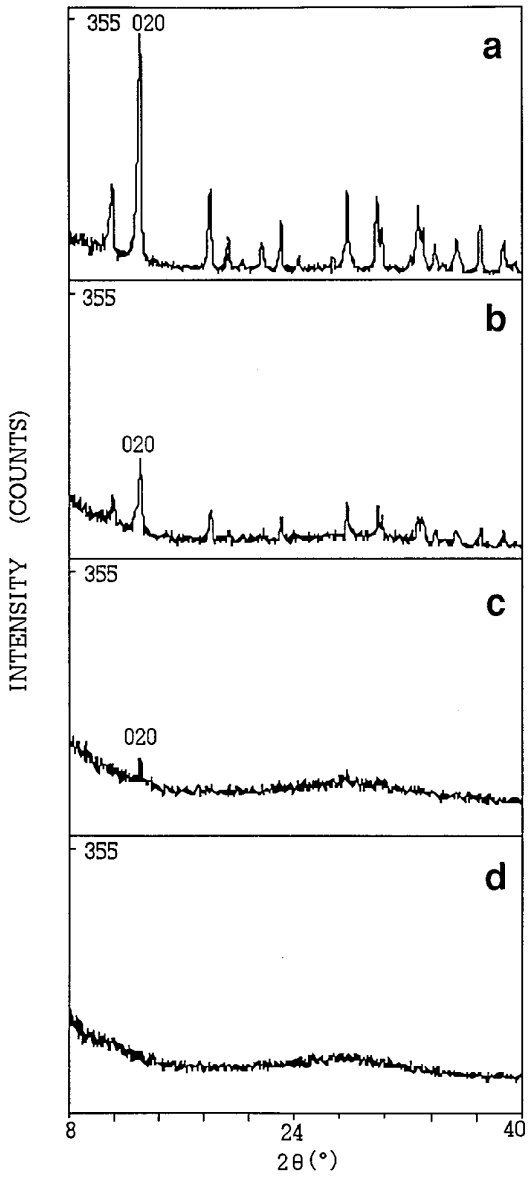

FIG. 6. X-ray diffraction spectra of the solids prepared with starting P/Fe ratio respectively equal to 1.5 (a), 2.5 (b), 3.5 (c), and 4.5 (d).

TABLE 3

P/Fe Atomic Ratio and Vivianite Content of the Precursors as a Function of the Initial P/Fe Ratio

Initial P/Fe atomic ratio	P/Fe atomic ratio of the precursor	Vivianite content (mol.%)[a]	
		Method 1	Method 2
1.5	1.03	93	81
2.5	1.60	35	44
3.5	2.07	14	14
4.5	2.30	0	0

[a] Calculated from chemical analysis data (method 1) and X-ray diffraction data (method 2).

4.3. Effect of the unreacted vivianite content of the precursors. It was observed that the formation of the precursor from the vivianite could be incomplete and that vivianite could remain in the precursor along with the amorphous phase. We have thus tested several precursors containing various amounts of vivianite. The results obtained are presented in Fig. 12. They show that the remaining vivianite

TABLE 4

Comparison of the Oxidation Extents, Determined Experimentally by Mössbauer Spectroscopy and Calculated from Chemical Analysis for Solid Synthesized with Different Initial P/Fe Ratios

Initial P/Fe ratio	$Fe^{3+}/(Fe^{3+} + Fe^{2+})$ Experimental (%)	$Fe^{3+}/(Fe^{3+} + Fe^{2+})$ Calculated (%)
1.5	30	32
2.5	47	56
3.5	60	69
4.5	80	80

TABLE 5

Catalytic Data of the New Catalyst and an Industrial Catalyst at 658 K, in the Oxidative Dehydrogenation of Isobutyric Acid

Catalyst	Selectivities (%) CO_2	PRO[a]	ACE[b]	MAA[c]	Rate of formation of MAA ($10^{-8} \cdot mol \cdot s^{-1} \cdot m^{-2}$)
New catalyst	2	8	16	74	960
Industrial catalyst	2	9	19	70	222

[a] Propene.
[b] Acetone.
[c] Methacrylic acid.

was not active nor selective and that no synergy effect could be observed between the unreacted vivianite and the phase $Fe_2(PO_3OH)P_2O_7$. The rate of formation and selectivity in MAA decreased regularly up to values corresponding to pure vivianite.

5. Characterization of the Catalysts

Under the conditions of catalysis the precursors underwent a transformation leading to a very active and selective crystallized solid. Most of the solids contained only one phase never shown to be present in iron phosphate-based catalysts until now. However in some cases α- and $\beta Fe_3(P_2O_7)_2$ were also observed. The parameters governing the presence of these phases and their effect on the catalytic properties of the catalysts is described elsewhere (22).

The X-ray diffraction spectrum of the catalysts were indexed with the orthorhombic cell parameters a = 9.722(9) Å, b = 10.833(9) Å, and c = 7.368(8) Å (Fig. 13). These parameters correspond to those calculated for the phase $Fe_2(PO_3OH)P_2O_7$ (23). The characterization of the catalyst by IR spectroscopy confirmed the presence of PO_3OH and P_2O_7 groups in the solid (Fig. 4b). These groups were characterized, respectively, by an intense band at 3498 cm^{-1} attributed to P–OH vibration and two bands at 725 and 775 cm^{-1} attributed to P–O–P asymetric vibrations (Table 1).

The structure of $Fe_2(PO_3OH)P_2O_7$ can be described by considering Fe_2O_9 units formed by two face-sharing FeO_6 octahedra. The dimers are interconnected by (PO_3OH) to

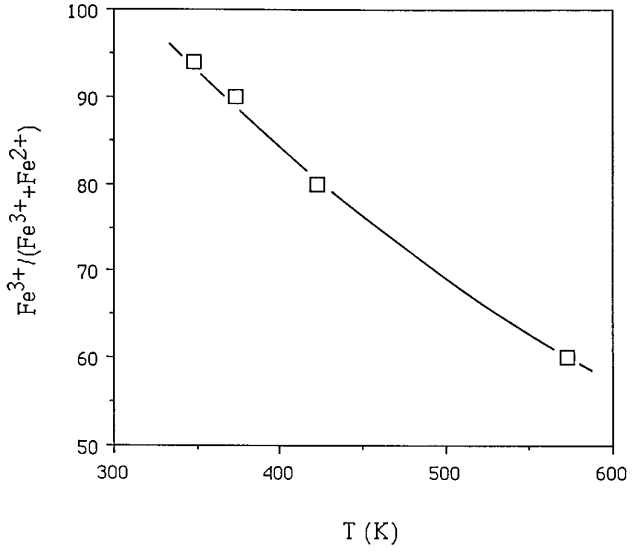

FIG. 7. Oxidation level of the solid ($Fe^{3+}/(Fe^{2+} + Fe^{3+})$) as a function of the rate of reflux varied with the temperature of the heating source.

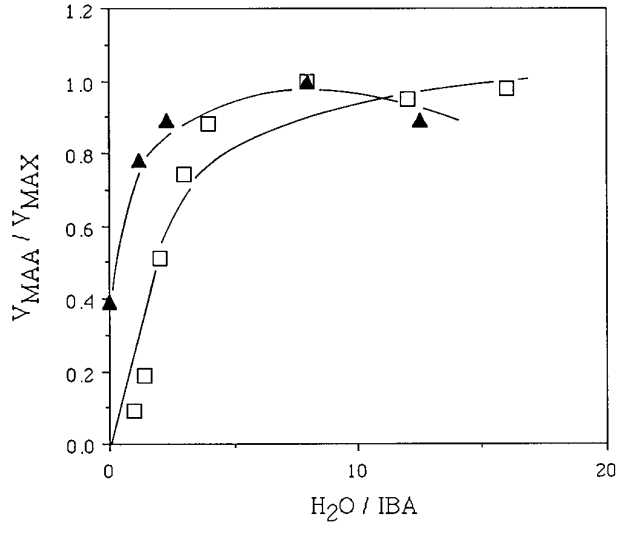

FIG. 8. Comparison of the ratio (R) of the rate of formation of MAA to the maximum rate as a function of the H_2O/IBA ratio for the new catalyst (▲) and the industrial catalyst (□).

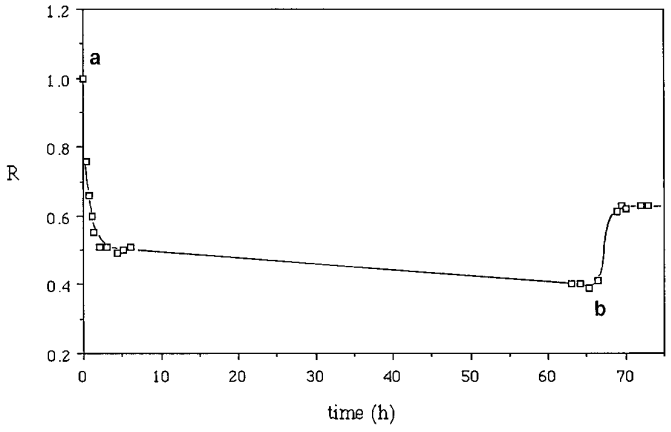

FIG. 9. Variations of the ratio of the rate of formation of MAA to the initial rate as a function of time with and without added water partial pressure; (a) stop of the water feed (72 kPa), (b) reestablishment of the water feed (72 kPa).

form sheets (plane *ac*) interconnected to each other by the (P_2O_7) groups (Fig. 14). Mössbauer spectra of a used catalyst is presented in Fig. 5b. It has been fitted to two doublets whose parameters are given in Table 2. These doublets could be assigned to one ferric site and one ferrous site. The ferric site presented an isomer shift characteristic of cations in a high spin state with an octahedral coordination and correspond to those characteristic of the phase $Fe_2(PO_3OH)P_2O_7$ (23). The ferrous doublet characterized by $\delta = 0.41$ mm $\cdot$ s^{-1} and $\Delta = 2.33$ mm $\cdot$ s^{-1} is present in relatively small quantities (relative spectral area varies between 1 and 7%). The quadrupolar splitting of this doublet is different from those observed for the other iron phosphates likely to be formed in the catalysts ($\alpha Fe_3(P_2O_7)_2$: $\Delta = 2.7$ mm $\cdot$ s^{-1}, $\beta Fe_3(P_2O_7)_2$: $\Delta = 4.2$ mm $\cdot$ s^{-1}, $Fe_2P_2O_7$: $\Delta = 2.6$ mm $\cdot$ s^{-1}). The thermic and thermogravimetric analyses of the catalyst showed two weight losses occuring between 573 and 723 K and 723 and 973 K. The mass spectrometry analysis performed simultaneously allowed us to attribute the first loss to the dehydration of the compound and the second to the decomposition of adsorbed hydrocarbon molecules. The first water loss corresponded to 0.49 mol of water for 1 mol of $Fe_2(PO_3OH)P_2O_7$, which is in agreement with the theoretical value corresponding to the total content of water of 0.50. XPS analysis results are reported in Table 7. Similar to what was observed before catalysis, the samples exhibited a large excess of phosphorus on the surface after catalysis, with a P/Fe ratio higher than that of the bulk. The P/O ratio was close to 0.25 which led us to propose that this was due to the presence of phosphate anions on the surface, as in the case of vanadium phosphate (24).

Figure 15 shows results of a high resolution transmission electron microscopic investigation of the catalyst. The solid appeared well crystallized from its electron diffraction pattern (Fig. 15a). The parameters calculated from the pattern were equal to 9.6 and 7.4 Å with an angle of 90° which corresponded relatively well to the *a* and *c* cell parameters. On the micrograph shown, the lattice fringes of 2.85 and 5.00 Å spacing are respectively of (2, 2, 0) (3.04 Å) and (1, 0, 2) (4.43 Å) planes of the structure of $Fe_2(PO_3OH)P_2O_7$ (Fig. 15b). The angle observed between these two plane families is about equal to 80°, a value close to the theoretical one (77°). Around the particles, an amorphous phase, the thickness, of which varied from to 2 to 6 nm, was systematically observed. Analytical electron microscopy experiments gave P/Fe atomic ratios for the

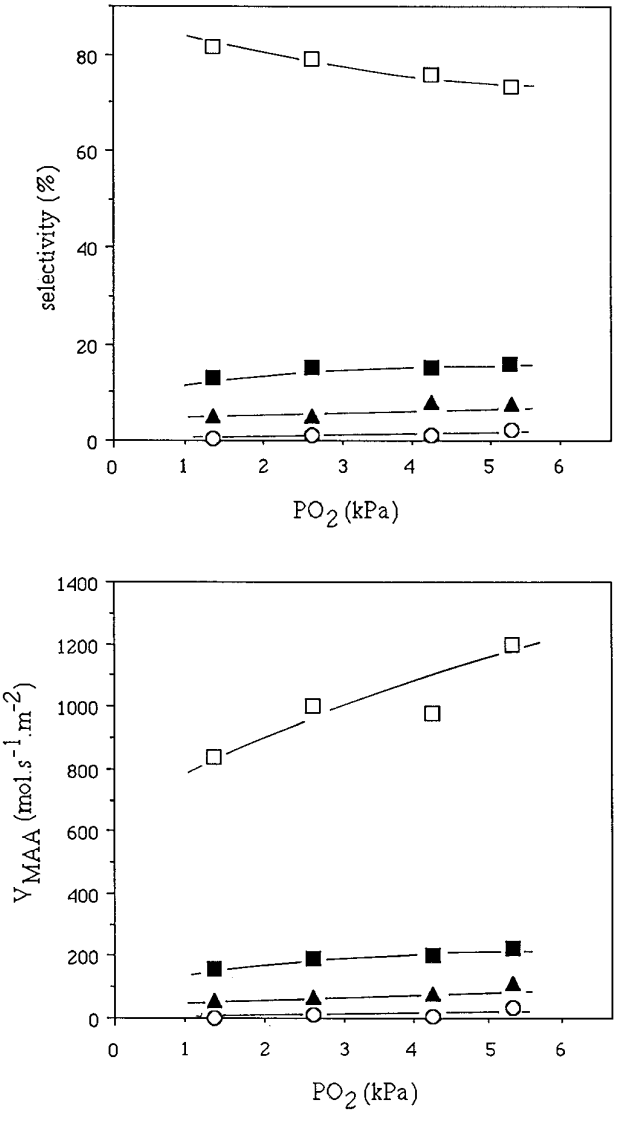

FIG. 10. Variations of the rates of the formation of the products (10^{-8} mol $\cdot$ s^{-1} $\cdot$ m^{-2}) and selectivities for IBA oxidative dehydrogenation at 658 K as a function of oxygen partial pressure; □MAA, ■ACE, ▲PRO, ○CO_2.

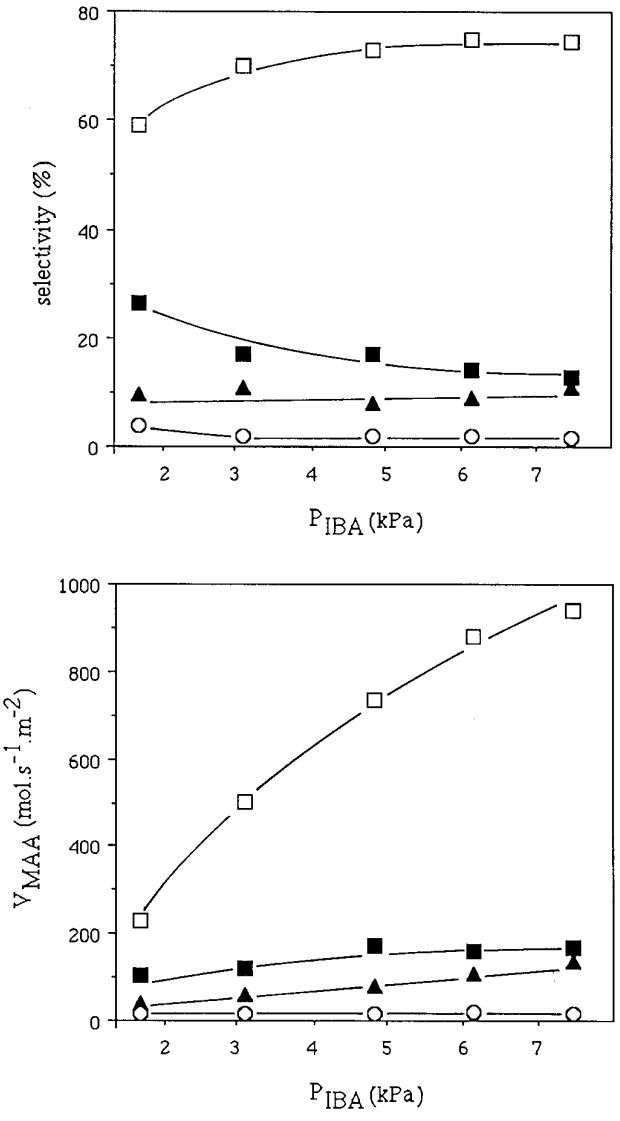

FIG. 11. Variations of the rates of the formation of the products (10^{-8} mol · s^{-1} · m^{-2}) and selectivities to MAA for IBA oxidative dehydrogenation at 658 K as a function of IBA partial pressure; □MAA, ■ACE, ▲PRO, ○CO_2.

particles with a relatively narrow distribution around 1.65 which is slightly higher than the relative ratio corresponding to the phase $Fe_2(PO_3OH)P_2O_7$. This discrepancy may be attributed to the excess of phosphorus located on the surface of the particles as evidenced by XPS (Table 7). From its structure it can be seen that $Fe_2(PO_3OH)P_2O_7$, as a well crystallized phase, cannot be reduced without important structural changes. Furthermore, this phase was the only crystallized phase shown to be present in the catalyst. It may thus be suggested that it is the amorphous phase observed by electron microscopy around the $Fe_2(PO_3OH)P_2O_7$ particles which contains the ferrous cations and that these cations were obtained under the reducing conditions of the reaction. The superficial amorphization of $Fe_2(PO_3OH)P_2O_7$ could either be due to this reduction or to the excess of phosphorus or to both. In order to confirm this hypothesis an analysis of the XPS data has been focused on the $Fe^{2p_{3/2}}$ peak obtained for two catalysts after the test, containing different Fe^{2+} content as determined by Mössbauer analysis, and for two pure phases, one ferrous and one ferric. It was possible to distinguish two peaks separated by approximately 2.5 eV, which could be attributed to ferrous and ferric cations (Fig. 16). The binding energies for $Fe^{2p_{3/2}}$ are listed in Table 8 together with the $Fe^{2+}/(Fe^{2+} + Fe^{3+})$ ratio calculated from XPS and Mössbauer spectroscopic data. The comparison of these ratios clearly showed that the ferrous cations were preferentially located at the surface of the solids. The amorphous phase should contain PO_3OH and P_2O_7 groups and may be $(Fe_3O_{12})^{16-}$ like in the active phase of the industrial catalysts instead of $(Fe_2O_9)^{13-}$. The great similarities observed in the catalytic properties between the two catalysts may support this hypothesis. It is interesting to note that the temperature range of the dehydration of $Fe_2(PO_3OH)P_2O_7$ is approximately the same as that of the active phase of the industrial catalysts, $\alpha Fe_3(P_2O_7)_2$ (7, 25): $Fe_2^{3+}Fe^{s+}(PO_3OH)_4 \rightarrow Fe_2^{3+}Fe^{2+}(P_2O_7)_2 + 2\ H_2O$ which was shown previously to occur around 673 K.

DISCUSSION

To synthesize the precursors, the use of both acetone and pyrophosphoric acid instead of other solvents like water, alcohol, toluene, and of other acids like orthophosphoric acid appeared to be essential to get the transformation of the vivianite in the amorphous precursor. This could be explained by the fact that the reaction involved $(H_xP_2O_7)^{x-4}$ anions and not $(H_xPO_4)^{x-3}$ and that these anions were stable in acetone but not in the other solvents (26). The transformation of the vivianite results in both an enrichment in phosphorus, the P/Fe atomic ratio of the

TABLE 6

Comparison of the Reaction Orders Relative to IBA and Oxygen for the Formation of Methacrylic Acid (MAA), Acetone (ACE) and Propene (PRO) Calculated with the New Catalyst and an Industrial Catalyst

Kinetic orders	MAA	ACE	PRO
	Relative to IBA		
New catalyst	0.90	0.35	0.80
Industrial catalyst	0.80	0.50	0.80
	Relative to oxygen		
New catalyst	0.20	0.25	0.50
Industrial catalyst	0.20	0.60	0.25

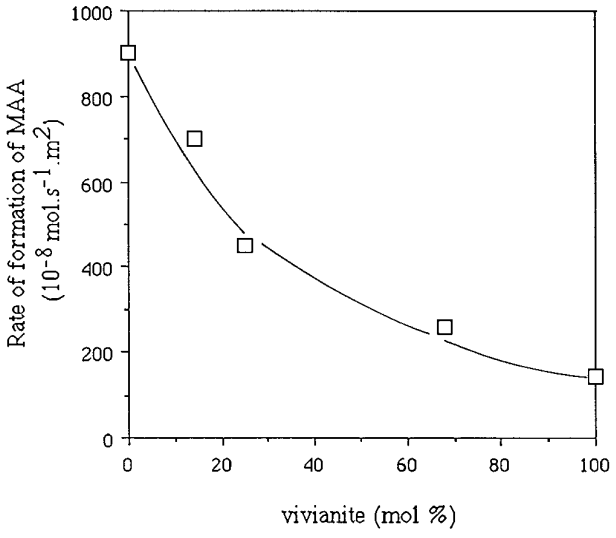

FIG. 12. Variations of the rates of the formation of MAA (10^{-8} $mol \cdot s^{-1} \cdot m^{-2}$) for IBA oxidative dehydrogenation at 658 K as a function of the molar percentage of vivianite in the catalyst precursors.

solid increasing from 0.66 to 2.3, and an amorphization. The fact that vivianite placed under reflux in acetone without pyrophosphoric acid was not transformed seems to indicate that these two features are related. The transformation rate of the vivianite appeared to depend upon the initial P/Fe atomic ratio and the morphology of the vivianite; this suggests that the transformation is controlled by kinetic parameters. It was also the case for the oxidation of the solid which was strongly affected by the rate of reflux used. It is possible that a competition occurred between the phosphorus enrichment of the vivianite and its oxidation, the oxidation rate being more strongly affected by the rate of reflux. The transformation of the vivianite also involved

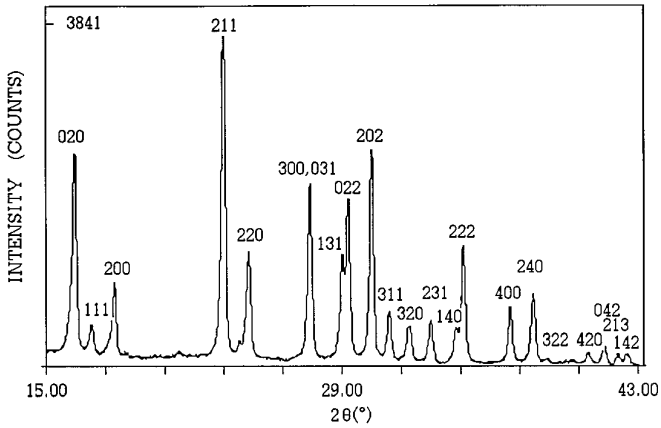

FIG. 13. Indeed X-ray diffraction pattern of the catalyst after the catalyst test at 658 K. The pattern was recorded with 16 s counting time per step. All indexed peaks correspond to $Fe_2(PO_3OH)P_2O_7$.

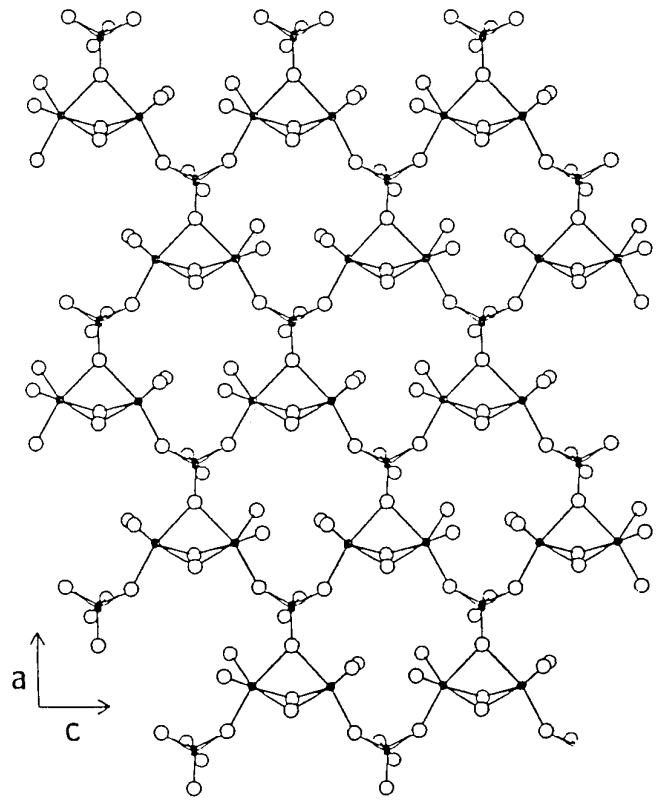

FIG. 14. Schematic representation of the structure of $Fe_2(PO_3OH)P_2O_7$ projected down [010] showing the interconnection between Fe_2O_9 and PO_3OH groups (23). Fe and P atoms are black dots and hydrogen atoms are not shown.

a change in morphology of the solid with the formation of uniform-size disks from thin platelets. The structure of vivianite is lamelar with sheets oriented parallel to the (010) plane (27). It may be postulated that the enrichment in phosphorus occurs between these planes which are bonded together only by hydrogen bonds.

Under the conditions of catalytic reaction all the precursors synthesized needed an activation period of approximately 48 h. During this time the solids underwent a total

TABLE 7

Atomic Ratios Calculated from XPS Data on the New Catalyst before and after Catalysis

	P/O	$Fe^{2p_{3/2}}/O$	$P/Fe^{2p_{3/2}}$
Before catalysis	0.37	0.11	3.2(2.3)[a]
After catalysis	0.25(0.20)[b]	0.09(0.13)[b]	3.90(1.5)[b]

[a] Ratio obtained from chemical analysis.

[b] Ratio corresponding to the stoichiometry of the phase $Fe_2(PO_3OH)P_2O_7$.

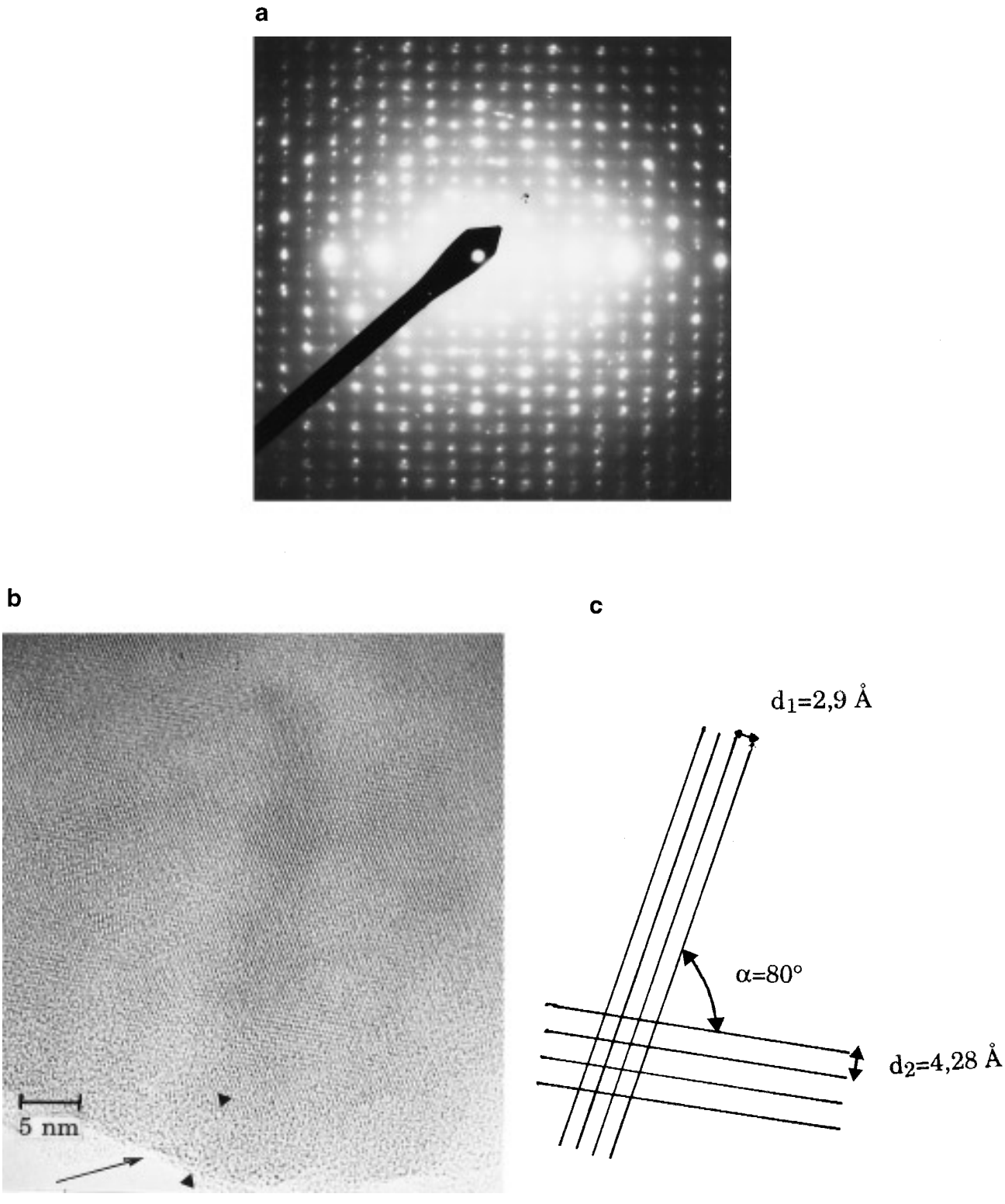

FIG. 15. High resolution transmission electron microscopic investigation of the new catalyst: (a) Electron diffraction pattern. (b) Transmission electron micrograph of the catalyst after the catalytic test at 658 K; the amorphous phase is shown by an arrow. (c) Enlarged schematic representation of the planes visualized on the micrograph.

transformation with a loss of phosphorus and the crystallization of a new phase. This new phase, identified as the $Fe_2(PO_3OH)P_2O_7$ phase, was much more active than the industrial catalyst with a slightly higher selectivity to MAA. It was shown in previous studies that the active and selective phase of the industrial catalysts was a mixed valence pyrophosphate $\alpha Fe_3(P_2O_7)_2$ (6, 7). It was suggested that this phase was, under the conditions of catalysis, oxidized and hydrated on its surface forming a phase of the type $Fe^{3+}_{3-x}F^{2+}_x(PO_3OH)_{3+x}(PO_4)_{1-x}$. It is interesting to note that the active and selective phase obtained with the new method of preparation is very similar to this phase. Both phases are made of (PO_3OH) groups and clusters of face-sharing ferric and ferrous octahedra. The active phase of the industrial catalyst consists of trimers of octahedra $(Fe_3O_{12})^{16-}$ while the catalyst used in this study consists of dimers $(Fe_2O_9)^{13-}$. The catalytic reaction could be written for the oxidized and hydrated form of $\alpha Fe_3(P_2O_7)_2$ (7, 25):

$$Fe^{3+}_3(PO_3OH)_3(PO_4) + x(CH_3)_2CHCOOH \rightarrow Fe^{3+}_{3-x}Fe^{2+}_x(PO_3OH)_{3+x}(PO_4)_{1-x} + x(CH_3)CH_2 = COOH \quad [1]$$

$$Fe^{3+}_{3-x}Fe^{2+}_x(PO_3OH)_{3+x}(PO_4)_{1-x} + x/4\ O_2 \rightarrow Fe^{3+}_3(PO_3OH)_3(PO_4) + x/2\ H_2O. \quad [2]$$

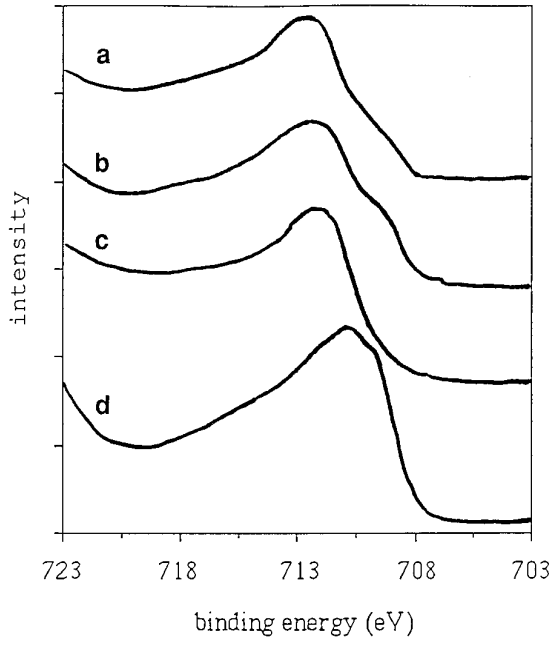

FIG. 16. Original XPS spectra of the binding energy range 703–723 eV showing the Fe photoelectron lines of two catalysts after catalysis with different oxidation extents ((a) catalyst 1 with 1% Fe^{2+}, (b) catalyst 2 with 5% of Fe^{2+}) and two pure phases ((c) $Fe_2P_2O_7$, (d) $Fe_4(PO_4)_3(OH)_3$).

TABLE 8

Comparison of Binding Energies for the Fe in Several Phosphates and Two Catalysts after Catalysis and Comparison of the Ratios Calculated from XPS and Mössbauer Spectroscopic Data

$Fe^{2p_{3/2}}$	Fe^{2+} (eV)	Fe^{3+} (eV)	$Fe^{2+}/(Fe^{2+} + Fe^{3+})$ XPS	$Fe^{2+}/(Fe^{2+} + Fe^{3+})$ Mössbauer
$Fe_2P_2O_7$	710	711.9	46	2
$Fe_4(PO_4)_3(OH)_3$	—	711.6	0	0
Catalyst 1	710	712.3	25	1
Catalyst 2	710.2	712.4	40	5

It can be seen that the species involved in the reaction were present on the surface of the new catalyst. This may explain why the new and the industrial catalysts exhibit similar selectivities for all the products, similar activation energies for their formation, and similar reaction orders toward oxygen and isobutyric acid. The fact that the new catalyst was slightly more selective in MAA and much more active than the industrial catalysts can easily be explained by the fact that the industrial catalyst contained, besides the active and selective phase, other phases with lower activity and selectivity. The observation that when no water was added to the feed the new catalyst was not rapidly and completely deactivated like the other catalysts but underwent a very slow deactivation can be explained by the fact that the new catalyst was hydrated in the bulk ($Fe_2(PO_3OH)P_2O_7$) while the others were hydrated only on the surface and that this feature allowed a better stabilization of the (PO_3OH) groups which are necessary to the reaction on the surface of the catalysts.

The study of the new catalyst without water showed that the catalyst deactivation had two causes. First, an irreversible deactivation occurred which could be due to the deposition of coke on the solid and which resulted in a loss of activity but not a loss of selectivity, the active sites being less numerous but not modified. Second, a reversible deactivation occurred which could be due to the reversible dehydration of the solid. We have proposed in previous studies that one of the major roles of water was to displace the following dehydration equilibrium to the left (25, 28): $(PO_3OH)_4 \rightarrow (P_2O_7)_2 + 2\ H_2O$). This dehydration, which occurs in the same range of temperature as the catalytic reaction, involves both a loss of activity and a loss of selectivity in MAA in favor of acetone and CO_2 according to a modification described elsewhere in a similar case for hydroxyphosphates (25).

ACKNOWLEDGMENTS

ELF-ATOCHEM is thankfully acknowledged for financial support and for supplying the industrial catalyst. This work is part of the ''Isobutyric Acid Oxidative Dehydrogenation Project Group'' (Groupement Scientifique du CNRS).

REFERENCES

1. Cavaterra, E., Petrini, G., Moreschini, L., Covini, R., Dalloro, L., and Pomodoro, P., assigned to Montedison, FR patent 74 27388, 1974.
2. Daniel, C., and Brusky, P. L., assigned to Ashland Oil Inc., FR patent 2 514 756, 1983.
3. Daniel, C., assigned to Ashland Oil Inc., EU patent 0 158 694, 1984.
4. Pedersen, S. E., Bremer, N. J., and Callahan, J. L., assigned to Standard Oil Inc., U.S. patent 4 427 792, 1984.
5. Ai, M., Muneyama, E., Kunishige, A., and Ohdan, K., *J. Catal.* **144,** 632 (1993).
6. Millet, J. M. M., Védrine, J. C., and Hecquet, G., *Stud. Surf. Sci. Catal.* **55,** 833 (1990).
7. Millet, J. M. M., Ph.D. Thesis, no. 259–90, Lyon, 1990.
8. Ai, M., Muneyama, E., Kunishige, A., and Ohdan, K., *Appl. Catal. A* **109,** 135 (1994).
9. Millet, J. M. M., and Védrine, J. C., *Appl. Catal.* **76,** 209 (1991).
10. Rouzies, D., Ph.D. Thesis, no. 48–92, Lyon, 1992.
11. De Wolff, P. M., *J. Appl. Crystallogr.* **1,** 108 (1968).
12. Rouzies, D., and Millet, J. M. M., *Hyperfine Interact.* **77,** 11 (1993).
13. Rouzies, D., Varloud, J., and Millet, J. M. M., *J. Chem. Soc. Faraday Trans* **90,** 2225 (1994).
14. Rouzies, D., Millet, J. M. M., Siew Hew Sam, D., and Vedrine, J. C., *Appl. Catal.* **24,** 198 (1995).
15. Virely, C., Fabregue, O., and Forissier, M., *Bull. Soc. Chim.* **3,** 457 (1988).
16. Dormann, J. L., Gaspérin, M., and Poullen, J. F., *Bull. Mineral.* **105,** 147 (1982).
17. Rouzies, D., and Millet, J. M. M., *Hyperfine Interact.* **77,** 18 (1993).
18. Detoni, S., and Hadzi, *Spectrochim. Acta* **20,** 949 (1961).
19. Hadzi, D., *Pure Appl. Chem.* **11,** 435 (1965).
20. Virely, C., Forissier, M., Millet, J. M. M., and Védrine, J. C. *J. Mol. Catal.* **71,** 199 (1992).
21. Dekiouk, M., Boisdron, N., Pietrzyk, S., Barbaux, Y., and Grimblot, *J. Appl. Catal. A* **90,** 61 (1992).
22. Bonnet, P., and Millet, J. M. M., to be published (1995).
23. Reiff, W. M., and Torardi, C. C., *Hyperfine Interact.* **53,** 403 (1990).
24. Agaskar, P. A., DeCaul, L., and Grasselli, R. K., *Catal. Lett.* **23,** 339 (1994).
25. Millet, J. M. M., Rouzies, D., and Védrine, J. C., *Appl. Catal.* **24,** 205 (1995).
26. Thilo, E., and Sauer, R., *J. Prakt. Chem.* **4,** 325 (1957).
27. Mori, H., and Ito, T., *Acta Crystallogr.* **3,** 1 (1950).
28. Védrine, J. C., Auroux, A., Coudurier, G., and Millet, J. M. M., ''Catalisis y Quimica Fina, Anales del Grupo Especializado de Catalisis.'' Series: Actas no. 16, Vol. 5, p. 237. Servicio de publicaciones de la Universidad de Cordoba, Cordoba, 1993.